

Article

Production and Properties of Electron-Beam-Welded Joints on Ti-TiB Titanium Alloys

Petro Loboda ¹, Constantine Zvorykin ^{1,*} , Volodymyr Zvorykin ¹, Eduard Vrzhyzhevskiy ², Tatjana Taranova ² and Valery Kostin ² 

¹ Igor Sikorsky Kyiv Polytechnic Institute, National Technical University of Ukraine, Prosp. Peremohy 37, 03056 Kyiv, Ukraine; decan@iff.kpi.ua (P.L.); vova.zvorykin@gmail.com (V.Z.)

² Paton Electric Welding Institute of the National Academy of Sciences of Ukraine, Kazymyr Malevych St. 11, 03150 Kyiv, Ukraine; ebw-30@ukr.net (E.V.); taranovatg@ukr.net (T.T.); valerykkos@gmail.com (V.K.)

* Correspondence: constantine.oleg@gmail.com; Tel.: +380-50-344-5292

Received: 10 March 2020; Accepted: 14 April 2020; Published: 18 April 2020



Abstract: In this article, structural features of Ti-TiB and ($\alpha+\beta$) Ti alloys in the initial state, in the weld and in the heat-affected zone of electron beam welds were investigated. The influences of welding parameters, such as influence of the electron beam velocity, preheating of the welded alloys and the subsequent annealing of the welded joint on the its microstructure, and the mechanical strength and ductility of the critical elements of the joint were studied by scanning electron microscopy using microprobe Auger spectral and X-ray diffraction analysis and tensile tests. It has been shown that the conditions for rapid crystallization of the material from the melt of the weld contribute to refining of reinforcing fibers of TiB and its hardening in comparison with the starting material Ti-TiB. Besides that, influences of the preferential orientation of TiB reinforcing microfibers (along and across the welded butt joint) on the mechanical properties of the welded joint were investigated by tensile testing. Using the methods of fractographic analysis, the effect of the boron-containing phase on the fracture character of Ti-TiB welded joints was established. It was shown that, along with the strengthening effect, TiB fibers cause embrittlement of the material.

Keywords: titanium alloys; titanium boride; microstructure; mechanical properties; welded joint; electron-beam welding; heat treatment

1. Introduction

The development of new titanium alloys for welded constructions is appealing. These alloys could be used in manufacturing engineering, allowing not only achieving high operational characteristics for constructions made from these alloys, but also increased economical effectiveness.

Titanium is characterized by low hardness, a high Young's modulus and relatively low ultimate strength (~480 MPa). This determines its limited usability in manufacturing in its pure form.

One of effective strengthening mechanisms of metal materials is reinforcement with high-module fibers. Composite metal-ceramic titanium alloys can be reinforced with high-melting compound fibers, such as titanium boride and silicide, which improve the strength by 2–3 times [1–7]. Such materials can be produced by using powder metallurgy. In such cases, high-melting compound fibers are mixed with titanium or titanium hydride powder or are synthesized during sintering of initially formed pressed parts from mixture of titanium hydride and high-melting powders. Another possibility to produce such strengthened alloys is introducing the strengthening fibers during crystallization of eutectic alloys. This ensures their uniform arrangement.

Strength of such metal-ceramic composites is determined by size and quantity of reinforcing fibers [8,9]. The size and quantity of titanium boride fibers during crystallization from eutectic alloys

of Ti-B system [10] are determined, first of all, by the temperature gradient at the crystallization front, the homogeneity of chemical composition in melt volume and the stability of thermal conditions (see Table 1).

For production of metal-ceramic composites with TiB fibers, electron-beam melting [11,12] or crucibleless zone melting [13] is used. Titanium is used as a matrix, and titanium boride as fibers, during the obtaining of a Ti-TiB based alloy [12,13].

Table 1. Mechanical properties of titanium and Ti-TiB alloy

Material	Yield Strength $\sigma_{0.2}$, MPa	Tensile Strength σ_t , MPa	Elongation δ , %	Reduction of Area Ψ , %	Vickers Hardness HV, MPa	References
Technical titanium	350–500	450–550	25	55	1400–2000	[12]
BT1-0	-	295–440	24–25	42–55	-	GOST 26492-85
Ti-TiB	631	882	13	16	3500–3700	[12]

Alloys of Ti-TiB type are cost-effective as they do not have to be alloyed with high-priced additions; besides, high-melting reinforcing fibers ensure high mechanical properties both at normal conditions, and under increased temperatures.

When using fiber reinforced alloys in constructions, similar joints between parts made from these alloys, and dissimilar joints between fiber reinforced Ti-alloys and other titanium alloys and mild steels are to be produced.

Generally, titanium alloys can be characterized by good weldability with each other [14–17], except for some of ($\alpha+\beta$)-alloys. The latter ones have a lower weldability, compared to α -alloys and β -alloys with stable structures, because they are more sensitive to the changes of the welding parameters. The required properties can be achieved through complex thermal treatment, which effects the base material and welded joint in different ways. Welding of titanium alloys is done mainly by electron-beam [18] or arc welding in argon [19]. Nevertheless, in case of welding Ti-TiB alloys, it is necessary to retain the structure of micro-reinforcing by TiB fibers. The new requirements for the weld formation conditions and the heat-affected zone (HAZ) have to be determined.

The present article presents basic options of welding parameter optimization for dissimilar joints of Ti-TiB_n alloys with other titanium alloys, and with other structural materials. The article shows the path to achieving high mechanical properties of welded constructions produced by electron-beam welding.

2. Materials and Methods

As our investigations focused on the influence of heat input during welding on the properties of Ti-TiB alloys [12], to keep the number of variables as low as possible, only one Ti-TiB alloy was investigated. The alloy was obtained by sintering powders of Ti (grade ПТК-1 ТУ14-22-57-92 (PTK-1 TU 14-22-57-92) fractional size 45–100 μm >85%, chemical composition, wt.%: N-0.07%, C-0.05%, H-0.35%, Fe-0.35%, Si-0.10%, Ca-0.08%, Cl-0.003%, Ti—the rest) and TiB₂ (fractional size ~ 5 μm , chemical composition (TU 113-07-11.040-89): Ti \approx 70%, B \approx 30%, Fe < 0.05% and C < 0.1%), which was carried out after mixing of Ti-95% and TiB₂-5% powders, pressing at $P = 0.65$ GPa and annealing in the β -area temperature range (sintering start temperature 1000 $^{\circ}\text{C}$, heating at a rate of 0.03 $\text{K}\cdot\text{s}^{-1}$ to 1200 $^{\circ}\text{C}$, 3 h, 10 Pa). Briquettes with a diameter of 30 mm and a height of 20 mm, which were obtained after sintering, were filled into the melting chamber of the electron-beam unit UE-208 (УЭ-208, Pilot Paton Plant, Ukraine). The briquettes were melted under a vacuum of $(7-9) \times 10^{-2}$ Pa in a crucible; then the melt was poured into a water-cooled copper crystallizer with a diameter of 110 mm. In the mold, a directed heat sink was achieved by heating the melt surface with electron beams of two electron guns with a heating spot diameter of 35–40 μm (scanning speed 5 $\text{mm}\cdot\text{s}^{-1}$). The surface of the ingot was kept in a molten state, forming a temperature gradient that provided directional crystallization with the formation of boride fibers, as described in [12]. After machining the ingot with removing a 2.5 mm layer, multiple deformation processing was performed on a Skoda 500/350 rolling mill with $\varepsilon = 20\%$

degree of plastic deformation. The final blank thickness for the experimental samples was 10 mm. The blanks for welding investigations were then extracted by water-jet cutting. The ends of the cut of the samples were ground to ensure parallel joint of the welded surfaces, so that the resulting surface roughness R_a was less or equal to $3.2 \mu\text{m}$.

The resulting microstructure of a Ti-TiB alloy, consisting of Ti-matrix with boride fibers, can be seen in Figure 1. The quantitative ratio of the phases Ti-95%, TiB₂-5% in the experimental samples was controlled by quantitative X-ray phase analysis by the RIR method.

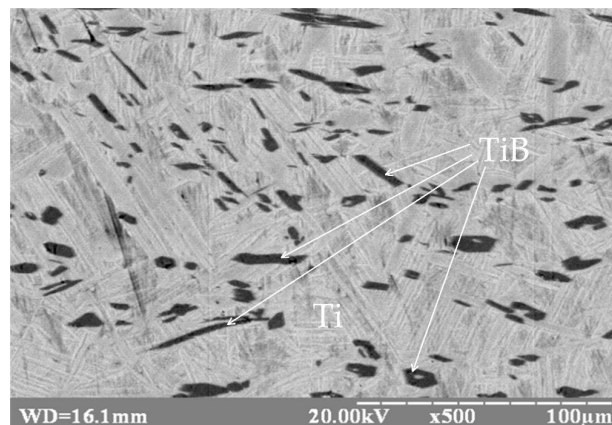


Figure 1. Structure of Ti-TiB melt before welding.

The metallographic analysis showed that TiB microfibers were uniformly distributed over the entire volume of the titanium matrix (α -Ti); their thickness was $2\text{--}7 \mu\text{m}$ (see Figure 1); and the fiber length ranged from $8 \mu\text{m}$ up to $70 \mu\text{m}$. The thickness of TiB fibers was correlated with their average length in a ratio of 1:3.

Ti-TiB can be classified as an alloy, as all of its components go through the stages of melting and subsequent crystallization with the formation of a structural reinforcing TiB phase in the form of reinforcing fibers.

In order to obtain the welded samples on bases of Ti-TiB alloy, electron-beam welding was carried out. Samples in the form of a parallelepiped with size $50 \text{ mm} \times 100 \text{ mm} \times 10 \text{ mm}$ were fixed in a clamp and welded at a longer face. The welding was carried out in the following mode of operation: $U_{\text{acc}} = 60 \text{ kV}$, $I_{\text{eb}} = 90 \text{ mA}$. Electron beam movement velocity was changed as $v_{\text{eb}} = 7, 10$ and $13 \text{ mm}\cdot\text{s}^{-1}$. For welding titanium alloys, the ellipse of the electron beam $3 \text{ mm} \times 4 \text{ mm}$ was located with its shorter diameter transverse to the welded joint. The scanning frequency of the electron beam was 170 Hz . The focus was on the weld surface. The diameter of the focused beam was 0.8 mm . The focusing lens current was 960 mA . A lanthanum-boride (single-crystal LaB_6) T-shaped cathode with a diameter of 3 mm was used. The distance from the electron gun to the weld butt was 70 mm . Electron-beam welding was carried out on UL-144 (УЛ-144, Pilot Paton Plant, Ukraine) welding machine.

The thermal source, ensuring the melting of contact zone of welded alloys, was the electron beam. Said beam was formed by an electron gun and was focused onto joint area of welding materials. Under close density of welding materials, the electron beam penetrates into the subsurface area in which they dissipate their energy. The depth of such a layer depends on the accelerating voltage and density of material to be processed, and may be evaluated by formula:

$$\Lambda = 2.35 \times 10^{-12} U_{\text{acc}}^2 / \rho, \quad (1)$$

where Λ is electrons penetration depth in μm , and ρ is density of material subjected to welding in $\text{g}\cdot\text{cm}^{-3}$. Thus, for a titanium alloy with density of $4.5 \text{ g}\cdot\text{cm}^{-3}$ under $U_{\text{acc}} = 60 \text{ kV}$, the value of $\Lambda \approx 20.5 \mu\text{m}$ —calculated using the Equation (1). Effective efficiency factor during the electron-beam welding has the values $\approx 0.85\text{--}0.95$.

In investigations presented in this article, the power density was $\sim 10^6 \text{ W}\cdot\text{cm}^{-2}$. In this power density range the electron-beam energy impact is characterized by melting penetration; the penetration depth to width ratio was 10:1 and more. The melting of the welded materials was complete with the formation of a vapor-gas channel at the point of interaction of the electron beam with the metal surface. The maximum metal temperature in the melt zone was $\approx 2200\text{--}2300 \text{ }^\circ\text{C}$ [14], which is much higher than melting temperature of titanium and TiB [20].

Specimens of the welded joints' cross sections of welded joints for metallographic investigations were extracted from the welded joints, using a precision water jet cutter KGA 2-R-2500 (Private Enterprise "Roden", Ukraine) by cutting across the weld, with subsequent grinding and polishing. Specimens were then etched with a solution 15%HF + 55% H_2O + 30% HNO_3 . Prepared surface layers were photographed and analyzed using a scanning electron microscope (by the JSM-840, JEOL Ltd., Japan) and REM-106I (PЭM-106И, OJSC "SELMИ", Ukraine, Sumy) scanning electron microscopes) and a probe for micro X-ray spectral and Auger spectral analysis with up to $\times 5000$ magnification. The pictures were obtained from secondary (SE) and back-scattered (BSE) electrons. The JAMP-9500F (JEOL Ltd., Japan) scanning electron microscope with the OXFORD EDS INCA Energy 350 (OXFORD INSTRUMENTS INDUSTRIAL PRODUCTS LIMITED, Abingdon, Oxfordshire, UK) energy-dispersive Auger-spectrometer was also used.

Tensile tests were carried out on a ZD-4 (VEB WERKSTOFFPRUFMASCHINEN, Germany, Leipzig) tensile testing machine according to the standard GOST 1497-84. Specimens for tensile test were water cut from the welded plate perpendicular to the weld axis so that the weld was in the middle of the tensile specimen and then machined to achieve the geometry shown in Figure 2. At least 6 samples were used for confirmation of results repeatability in the experimental cycle.

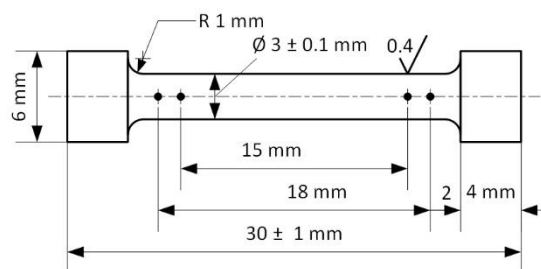


Figure 2. Tensile test specimen sketch—test specimens were manufactured according to GOST 1497-84 (ISO 6892-84).

X-ray structural investigations of the samples were carried out by the DRON-UM-1 (ДРОН-УМ-1, IC "Bourestnik", Russia) X-ray diffractometer in copper $\text{K}\alpha$ -radiation by step-scan method [12].

3. Results and Discussion

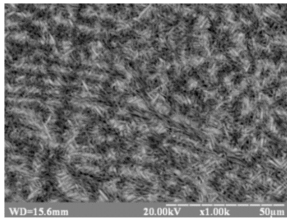
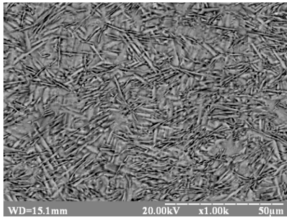
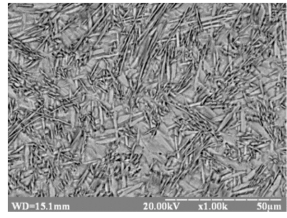
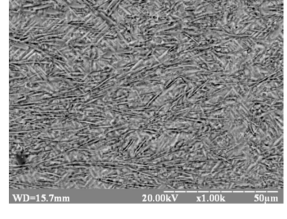
3.1. Welding of Similar Joints Ti-TiB Alloy

3.1.1. Influences of Welding Parameters on Microstructure and Mechanical Properties

In Ti-TiB alloy, the TiB phase, which is known to embrittle the material, leads to a hardening and forms the composite microstructure. This explains the expediency of retaining of microstructure with TiB reinforcing fibers in the welding zone being formed. In the investigations [12,13], it was shown that under conditions of zone melting the reinforcing TiB fibers are formed predominantly elongated in direction of crystallization-front movement. In overheated areas diboride inclusions are formed, which are more faceted and which capture the boron necessary for formation of titanium monoboride reinforcing fibers. This is essential during the selection of parameters of heat input into the weld.

Parameters of electron-beam welding were varied, as shown in Table 2; their influences on microstructure and mechanical properties were determined.

Table 2. Characteristics of the materials of Ti-TiB welded joints produced under various modes of electron-beam welding.

No. of Sample Series	Electron Beam Movement Velocity, v_{eb} , $\text{mm}\cdot\text{s}^{-1}$	Initial Temperature of Welded Materials, T_0 , °C	Logged Phases	Crystal Lattice Distortion, Δ , %	Average Size of Crystalline Blocks, $\bar{\Pi}$, 10^{-10} m	Mechanical Characteristics				Material Metallographic Structure in Welded Seam Area
						Yield Strength $\sigma_{0.2}$ MPa	Tensile Strength σ_t Mpa	Elongation δ %	Reduction of Area Ψ %	
1	7	20		α Ti-0.1 TiB-0.209	α Ti-150 TiB-56.36	957.2	1040	2.0	6.6	
2	10	20	α Ti TiB	α Ti-0 TiB-0.23	α Ti-142 TiB-195.1	-	1023.1	-	-	
3	13	400		α Ti-0 TiB-0.004	α Ti-141 TiB-84.03	-	950.2	-	-	
4	13	20		α Ti-0.2 TiB-0.41	α Ti-140 TiB-86.65	-	950	-	-	

For the material of welded joint, three typical zones can be defined (see Figure 3):

- Base material hardly influenced by welding process;
- Weld metal which is formed from the melt;
- Transient zone which is formed during the melt's interaction with the base material.

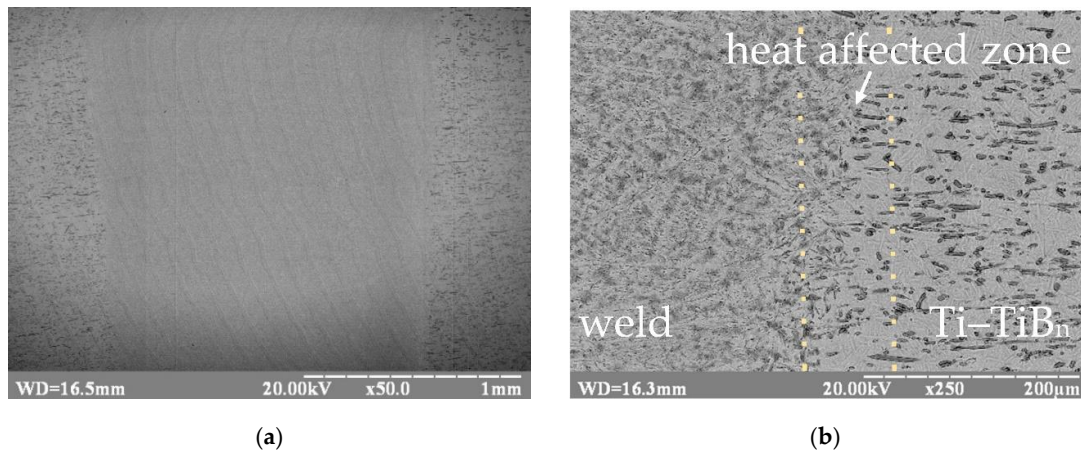


Figure 3. Welded joint produced by electron-beam welding of Ti-TiB_n samples: (a) overview; (b) microstructure of weld metal, heat-affected zone (HAZ) and base metal.

The metallographic analysis shows that the structure of base material and that of the one obtained in result of welded seam formation differ considerably (see Figures 1 and 4).

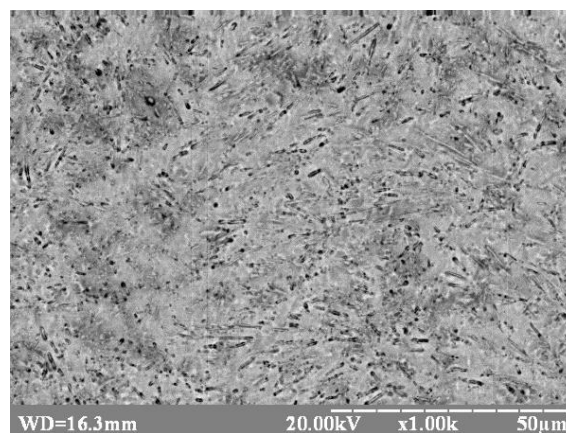


Figure 4. Typical structure of Ti-TiB alloy in the weld metal after welding.

In the welded seam zone, significant changes in structure of welded material were observed (Figure 4), compared to the unaffected base metal (see Figure 1). The microstructure of welded seam material has patterns typical for formation under conditions of fast crystallization of Ti-TiB melts (Figure 5).

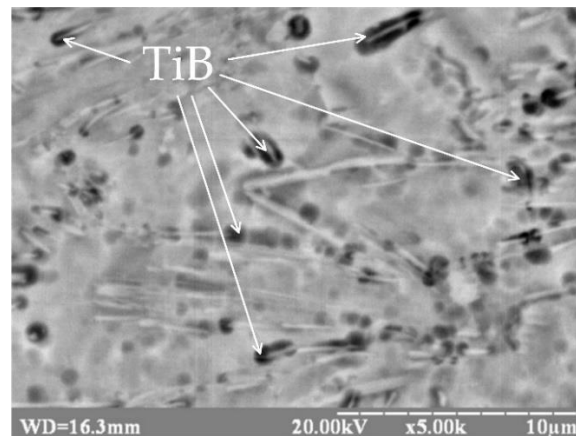


Figure 5. Distribution of boron-containing fibers in weld metal.

The main characteristics of the material revealed in the welded seam area, can conditionally divide the area into three zones (see Table 3).

Table 3. Characteristics of Ti-TiB_n structure (by results of phase X-ray structural investigations, $n = 1$) in the welded seam zone.

No. of Sample Series	Heat Affected Zone (See Figure 6). Area, Retaining the Structural Peculiarities Both Base Material, and Weld Metal	Weld Metal (See Figure 7)	Base Material
1	Zone width is 50 µm on average. In the material are areas without fibrous inclusions, and areas engaging both initial large TiB fibers, and thin micron and submicron fibers.	TiB fibers have not predominant orientation (see Figure 6a). Fibers length is from 2 to 8 µm. TiB fibers thickness is correlated with their length in proportion from 1:4 to 1:8 on average. Average distance between fibers in Ti matrix is 1.5 µm.	It is typical the presence of large elongated grains of titanium boride, for which is typical the decrease of peak intensity of titanium characteristic X-ray emission by 1.2–1.3 times in comparison with the main titanium matrix. Fibers are distributed uniformly by whole volume (their thickness is 2–7 µm (see Figure 2)), fibers with length from 8 to 70 µm are observed. TiB fibers thickness is correlated with their length in proportion 1:3 on average, at that, this proportion for various inclusions is vary from 2:3 to 1:15. Orientation of reinforcing fibers is initial.
2	Zone width is 40 µm on average. In the material are areas without fibrous inclusions, and areas engaging both initial large TiB fibers, and thin micron and submicron fibers.	TiB fibers have not predominant orientation (see Figure 6b). Fibers length is from 1 to 4 µm. TiB fibers thickness is correlated with their length in proportion 1:5 on average, at that, this proportion for various inclusions is vary from 1:4 to 1:6. Average distance between fibers in Ti matrix is 0.8 µm.	
3	Zone width is 32 µm on average. Feature of structure in such transient zone in comparison with samples Nos. 1, 2 and 4 is more high degree of homogeneity which is approaching to the characteristics of welded seam material.	TiB fibers have not predominant orientation (see Figure 6c). Fibers length is from 5 to 20 µm. TiB fibers thickness is correlated with their length in proportion 1:9 on average, at that, this proportion for various inclusions is vary from 1:4 to 1:11. Average distance between fibers in Ti matrix is 4 µm.	
4	Zone width is 28 µm on average. In the material are areas without fibrous inclusions, and areas engaging both initial large TiB fibers, and thin micron and submicron fibers.	TiB fibers have not predominant orientation (see Figure 6d). Fibers length is from 2 to 6 µm. TiB fibers thickness is correlated with their length in proportion 1:10 on average, at that, this proportion for various inclusions is vary from 1:6 to 1:10. Average distance between fibers in Ti matrix is 0.8 µm.	

The results obtained testify the increasing of zone width, formed during interaction of the melt with the sample crystal metal, both under decrease of electron beam movement velocity, and under increase of temperature of the welded samples. This is evidence of the development of relaxation thermodynamic processes in the boundary zone. Completeness of their passing demands availability of a long-time interval and increased temperatures.

The initial temperature and movement velocity of the electron heating source affect the development of relaxation processes in a different way. Under a preheating temperature of 400 °C, a considerable increase of boron-containing phase homogeneity distribution in transient zone and an increase of fiber length and thickness were observed, compared to non-preheated samples. Decrease of the electron beam movement velocity led to a decrease of fiber dimensions, and their distribution in the transient zone became more heterogeneous and had dendritic character.

The metallographic analysis showed that the structures of the initial material and the one obtained in the result of welded seam formation differ considerably (see Figures 6 and 7).

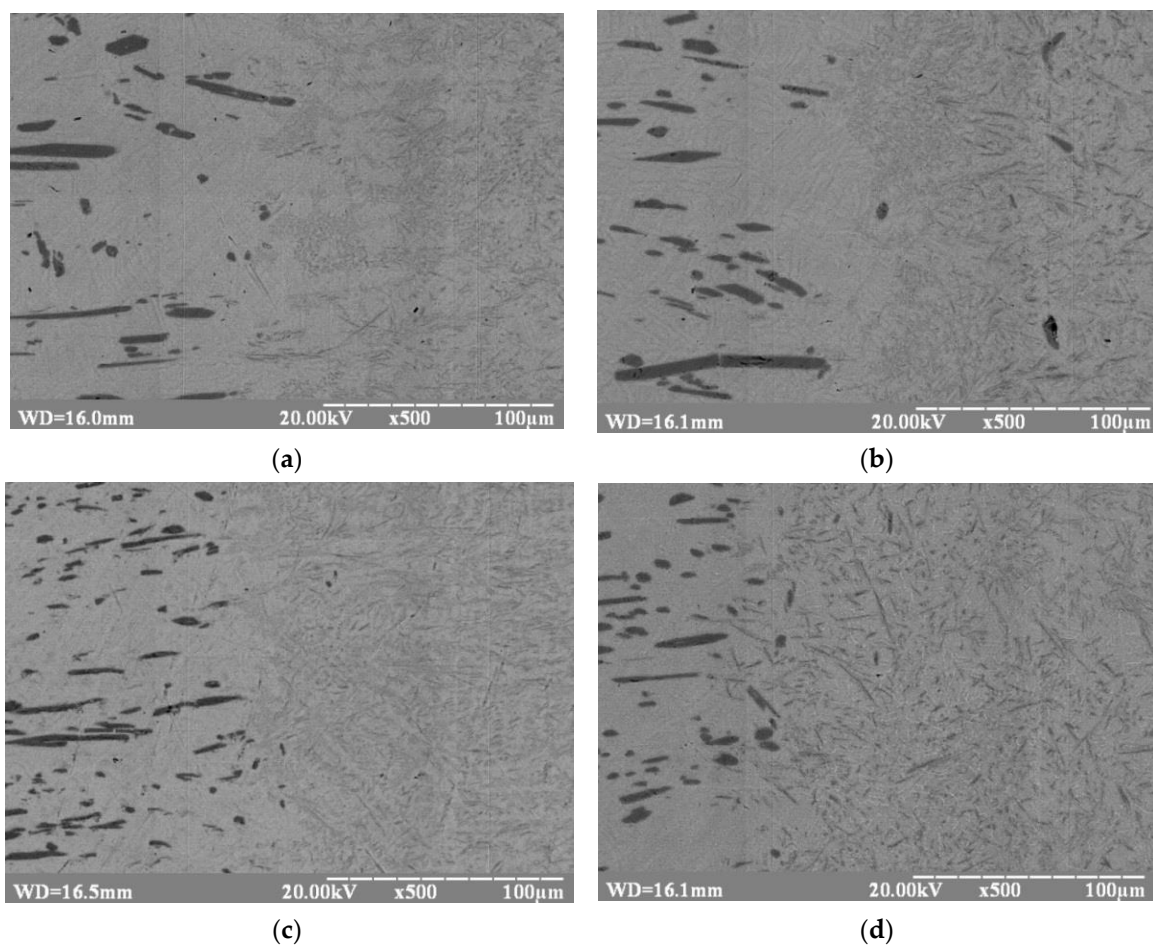


Figure 6. Structure of the material in the area of base material transition into weld metal: (a) sample of number 1 series; (b) sample of number 2 series; (c) sample of number 3 series; (d) sample of number 4 series.

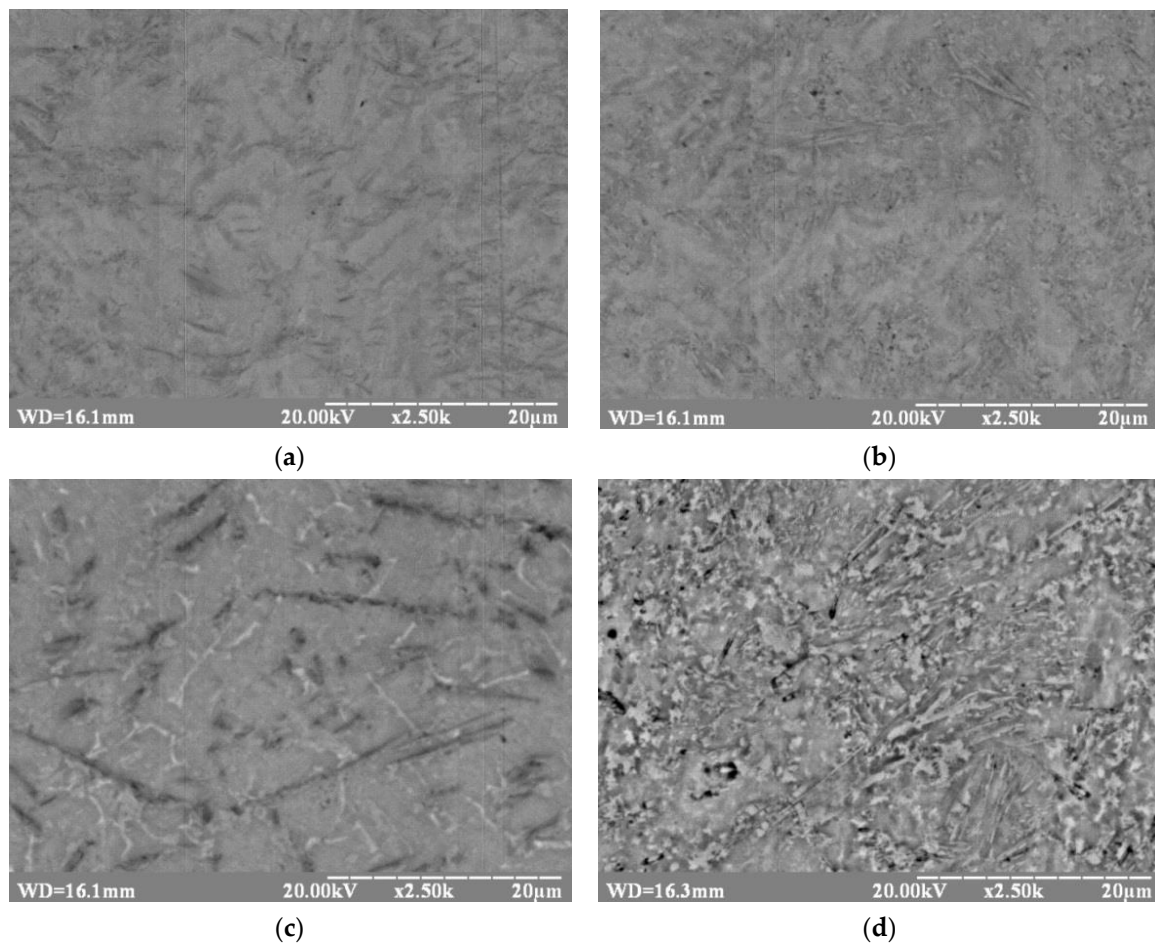


Figure 7. Structure of Ti-TiB alloy in the weld metal after electron-beam welding: (a) sample of number 1 series; (b) sample of number 2 series; (c) sample of number 3 series; (d) sample of number 4 series.

In the weld metal, formed by crystallization from the melt, similar trends are observed (see the Figure 7). At the same time, the smallest dimensions and largest uniformity of TiB fibers distribution in TiB matrix are observed in weld metal at medium value of electron beam movement velocity $v_{eb} = 10 \text{ mm}\cdot\text{s}^{-1}$. Preheating of parts subjected to welding results in considerable increase of TiB fibers' dimensions, which is due to increase of total specific internal energy of material in the zone. Obviously, the increase of v_{eb} results in a considerable increase of temperature gradients, and correspondingly, in essentially greater non-equilibrium of phase and structural states. During v_{eb} increase, the following changes of material structure in the transient zone were observed:

- Segregation of boron-containing fibers in areas with their increased content and formation of areas depleted with such phases (see Figure 6a).
- Growth of boron-containing fibers both by length, and by thickness, upon increasing of residual temperature of joint subjected to welding both at the expense of the electron beam impact increase (see Figure 7a), and at the expense of preliminary heating (see Figure 7c). At that, the effect of preliminary heating is displayed to a considerably greater extent.

Results of mechanical breaking tests of Ti-TiB welded samples demonstrated that material structure in weld metal, and mechanical properties of welded joints and base material, depend on welding parameters (see the Table 2). Particularly, at the minimum velocity of electron beam movement, it was possible to obtain some level of plasticity.

3.1.2. Fractographic Investigations

Fractographic investigations and analysis of fracture zone location regarding to the welded seam of Ti-TiB series welded joints have demonstrated that all samples were fractured by base material. This is evidence of the fact that the strength of welded joint is not less than the strength of the base material (see Figure 8).

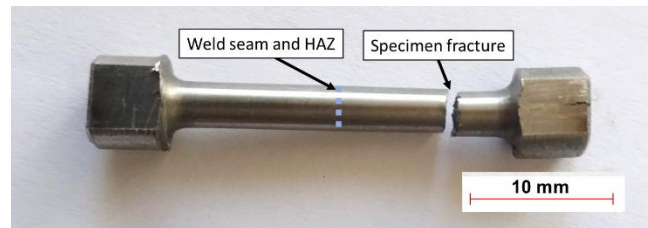


Figure 8. General view of fractured Ti-TiB welded specimen.

During tensile tests of Ti-TiB welded joints it was revealed that under a welding temperature change from 20 to 400 °C the maximum strength and plasticity were observed with the minimum velocity of electron beam movement. At that, the mixed character of the fracture was observed. Fragments of ductile fractured, light-colored wave combs (see Figure 9) were observed on the fracture surface, and the fracture was mainly of trans-crystalline type, as determined by its brittle cleavage mechanism.

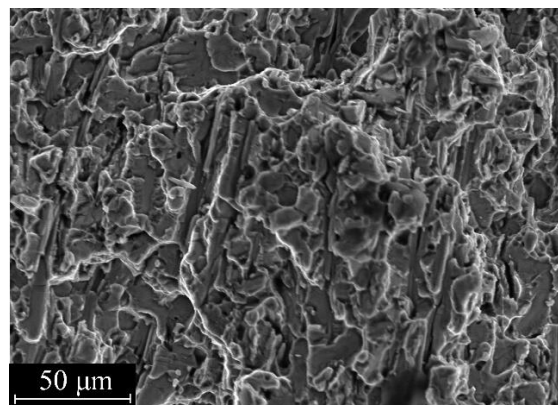


Figure 9. Fractographic investigation of Ti-TiB titanium alloy welded joint produced by electron-beam welding, $\times 500$.

In Figure 9 the fracture area is presented, in which one can see that large rod borides are cracked because of high stresses arising around them, which results in brittle fracturing. Shorter borides (less than 5 μm) do not result in strong localization of stresses, and thus, do not significantly affect the fracture toughness of a plastically deformed matrix. In the Figure 9 the fragment with brittle fracturing is presented, wherein the secondary cracks are revealed on the fracture's surface, which are localized frequently in area near boride inclusions.

Because the welded construction fracturing takes place via the base material, the influences of varied welding parameters may be attributed to the thermal influence on the base material. Minimum distortion of the titanium boride crystal lattice and minimum dimensions of TiB crystalline blocks are observed at minimum velocity of electron beam movement (see the Table 2). Lesser distortion of titanium boride crystal lattice is observed under preliminary heating only, but it results in a considerable increase of mean TiB crystalline block size. According to the results of [10], high adhesive strength of interphase boundaries between titanium matrix and TiB filamentary crystals in VT18U/TiB composites is retained up to the temperatures $T = 600\text{--}700$ °C. Initial heating up to 400° C may result in exceeding these temperatures in the heat-affected zone, and as a consequence, the breaking of adhesion bonds in

some areas of large TiB crystalline blocks along with occurrences of additional defects, which promote brittle fracture and strength lowering.

3.2. Welding of Dissimilar Joints between Ti-TiB and $(\alpha+\beta)$ Ti Alloy

Influences of Welding Parameters and Heat Treatment on Microstructure and Mechanical Properties

In case of Ti-TiB welding with titanium alloy without reinforcing fibers, it is necessary to understand the way in which the transient zone of welded seam shall be formed and will it lead to lowering of its strength.

The $(\alpha+\beta)$ Ti alloy, in terms of its composition (Al-3.5%, Nb-3.0%, Fe-2.5%, V-1.9%, Mo-1.4%, Zr-1.3%, Si-0.1%, T—the rest), is close to the T110 alloy (5.0–6.0% Al, 3.5–4.8% Nb, 1.5–2.5% Fe, 0.8–2.0%, 0.8–1.8% Mo, 0.3–0.8% Zr, 0.09% O₂, 0.02% N₂, 0.003% H₂), which was developed jointly with the Paton Electric Welding Institute of National Academy of Sciences of Ukraine and “Antonov” State Enterprise (patent of Ukraine number 40087C2 of 16.06.2003) and which is characterized by sufficiently high mechanical properties.

For alloys of Ti-TiB type, the anisotropy of mechanical properties, determined by directionality of reinforcing fibers, is typical. In the Table 2 the mechanical properties of welded joints of Ti-TiB with T110 type alloy are presented, in which the initial orientation of TiB fibers in Ti has a predominant directionality that is perpendicular to the surface subjected to welding. It permits us not only to analyze the processes of production of Ti-TiB and the T110-type alloy welding joint, but also to carry out the analysis of the effects of the reinforcing fibers' orientation in the initial Ti-TiB alloy on the properties of the welded joint produced.

The welding was carried out in the following mode of operation: $U_{acc} = 60$ kV, $I_{eb} = 90$ mA, electron beam movement velocity $v_{eb} = 7$ mm·s⁻¹, beam sweep—elliptic, transversal (3 mm × 4 mm). After welding, some of the welded samples were subjected to annealing for 1 h at the temperature 750 °C (in air condition) or at the temperature 850 °C (in vacuum). Results of mechanical tests of Ti-TiB–T110 samples before and after thermal treatment are in the Table 4.

Table 4. Mechanical characteristics of welded joints of Ti-TiB alloy with T110 titanium alloy obtained by electron-beam welding.

No. of Sample Series	Kind of Welding Joint	Thermal Treatment	Mechanical Characteristics				Structure of Material in Weld Metal	Notes
			Yield Strength $\sigma_{0.2}$ MPa	Tensile Strength σ_t MPa	Elongation δ %	Reduction of Area Ψ %		
5	(Ti-TiB)–T110	Without annealing	918.9	991.5	1.2	2.3	Reinforcing fibers along the load axis	Fracture by T110 alloy
6		Without annealing	-	931.3	-	-	Reinforcing fibers across the load axis	Fracture by (Ti-TiB) alloy
7		Annealing 750 °C 1 h (air)	928.7	970.5	2.0	5.9	Reinforcing fibers are across	Fracture by (Ti-TiB) alloy
8		Annealing 850 °C 1 h (vacuum)	-	975.7	-	-	Reinforcing fibers are across	Fracture by (Ti-TiB) alloy

Regarding the beginning of the plastic deformation process before the fracturing of number 7 series samples, the results of fractometric analysis of fracture surfaces are in Figure 10. Peculiarities of the fracture surfaces of series 6 samples, characterized by $\sigma_t = 931.3$ MPa (see Figure 10a), and series 6 samples, characterized by $\sigma_t = 970.5$ MPa and $\delta \approx 2\%$ (see Figure 10c), permits us to confirm that in both cases the brittle fracture was initiated by developments of brittle cracks at the boundary TiB fiber–titanium matrix. This statement is supported by the fact that TiB fibers are found on all fracture

surfaces (see Figure 10b,d). An increase of the specific area of adhesion contact of TiB fibers with a titanium matrix within the total cross-sectional area of a specimen with transversal fiber orientation subjected to deformation, results in an increase of brittle-crack-nucleus development probability in such areas. On the fracture surfaces of series 7 samples, some traces of plastic deformation may also be observed (see Figure 11), which are absent in series 6 and 8 samples.

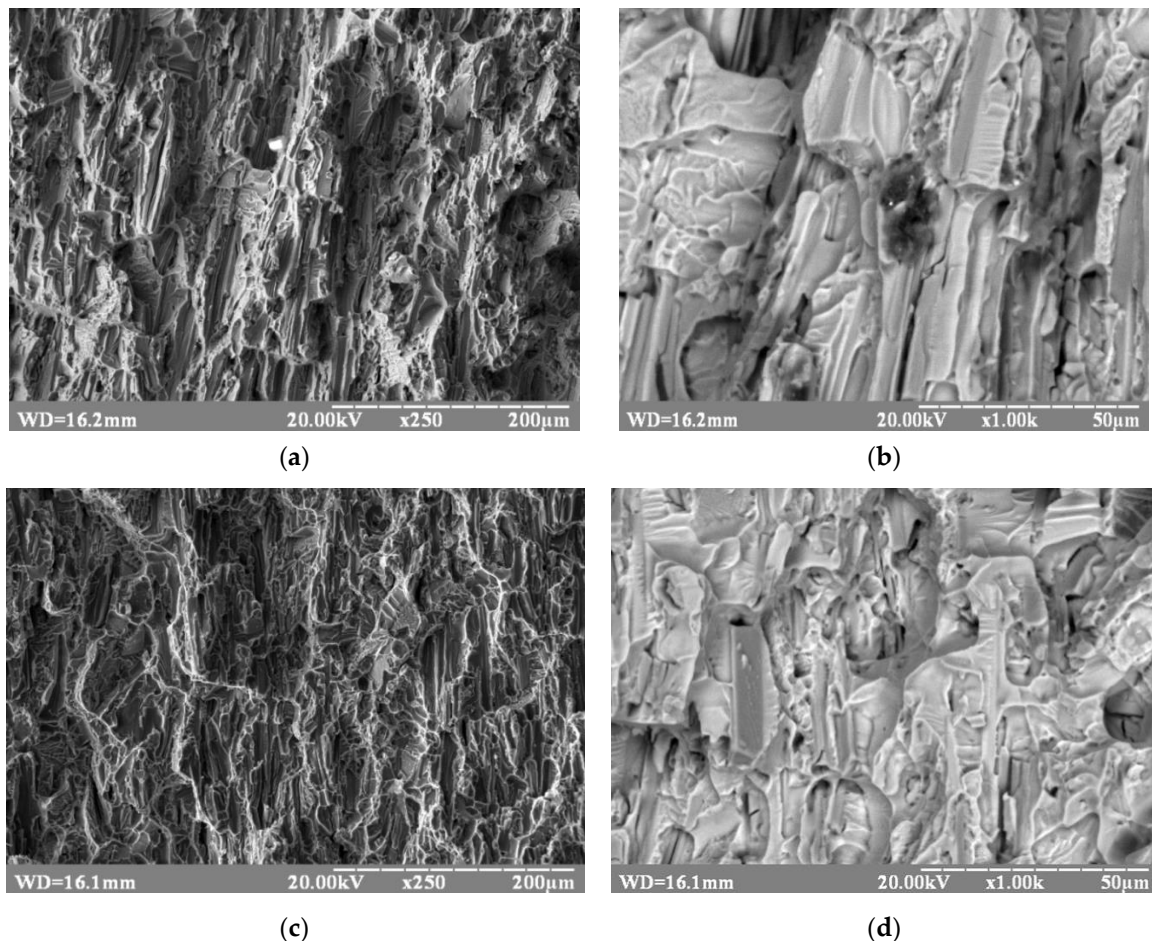


Figure 10. Structure of fracture surfaces of series 6 (a,b) and 7 (c,d) samples.

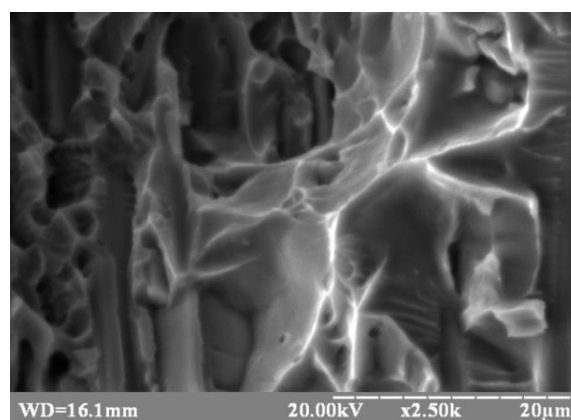


Figure 11. Cellular traces of plastic deformation on fracture surface of a series 7 sample.

In the welded samples, dark colored boron-containing inclusions were observed in the crystallization zone in which molten material contacted Ti-TiB alloy, which retained a solid state (see

Figure 12a). These inclusions have dimensions from submicron quasi-spherical, segregated into the boundary clusters, up to micron, which are close to initial TiB reinforcing fibers.

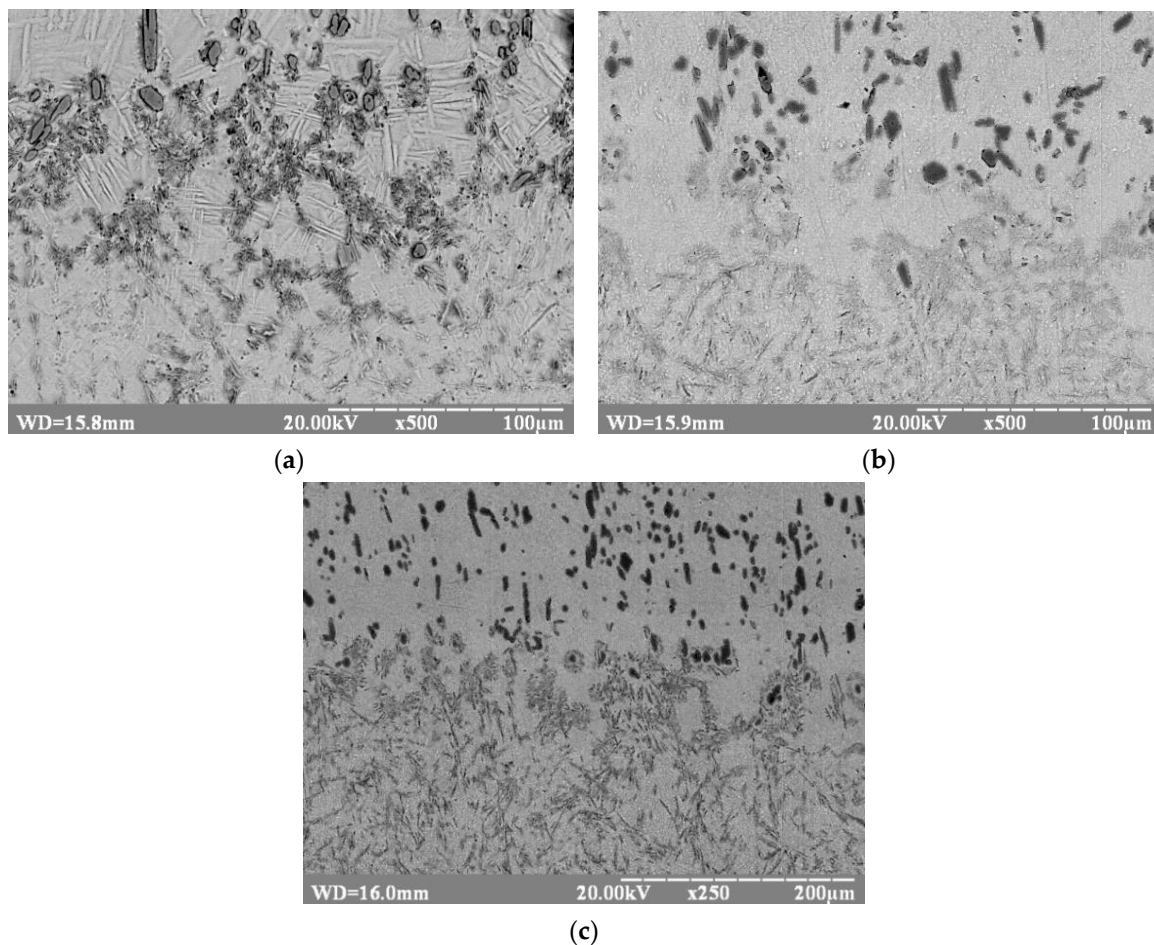


Figure 12. Microstructures of (Ti-TiB)-T110 welded joint material in Ti-TiB-welded seam zone: (a) number 6 series sample; (b) number 7 series sample; (c) number 8 series sample.

Annealing of specimens at 750 °C (see Figure 12b) and 850 °C (see Figure 12c) results in dissolution of the above-mentioned quasi-spherical clusters, while retaining the part of initial reinforcing TiB fibers (see Figure 13b). In such a boundary zone, the submicron TiB-reinforcing fibers are also formed (see Figure 14). After annealing at 750 °C they are distributed more uniformly and after annealing at 850 °C they form a cluster network, typical for all welded seam material (see Figure 15). Dissolution of boron-containing clusters in boundary zone of Ti-TiB-weld metal during subsequent short-term annealing can be considered a proof of thermodynamic instability of these formations. In the experiments [21] the presence of meta-stable Ti_2B was observed. It formed from Ti-B liquid phase at ~2200 °C and subsequently disappeared under conditions of thermodynamic stabilization at ~1800 °C. Very likely, under the conditions of electron-beam welding, rapid cooling at the boundary between Ti-TiB and molten metal resulted in fast crystallization in this zone and the formation of a meta-stable phase, which was dissolved during annealing at 750 °C and 850 °C (1 h).

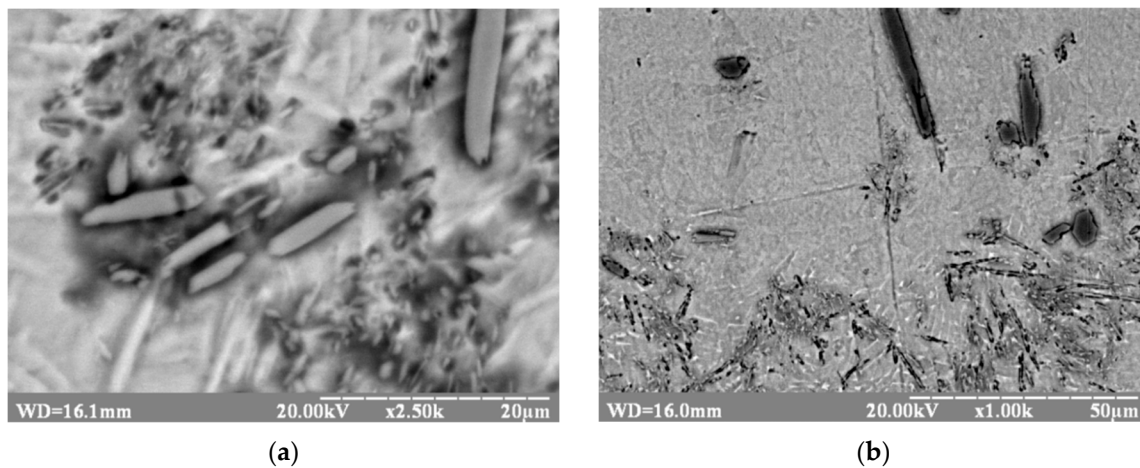


Figure 13. Boron-containing inclusions in the Ti-TiB welded seam zone of (Ti-TiB)-T110 welded joint: (a) after electron-beam welding (number 6 series sample); (b) after electron-beam welding and subsequent annealing at 850 °C (number 8 series sample).

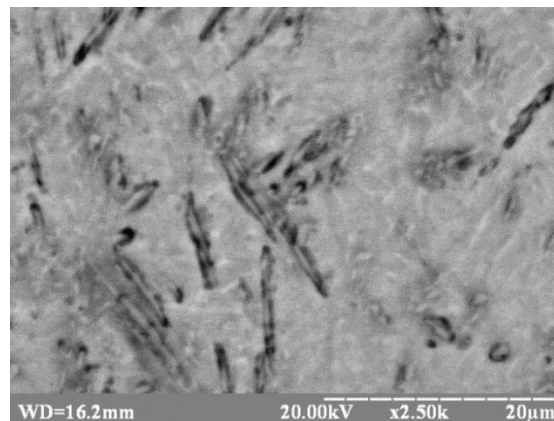


Figure 14. TiB submicron reinforcing fibers of (Ti-TiB)-T110 welded joint area in Ti-TiB-welded seam zone—after annealing at 750 °C.

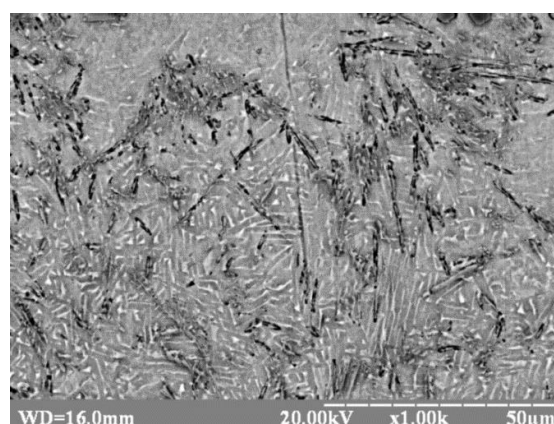


Figure 15. Network of TiB-reinforcing fiber clusters in Ti-TiB-welded seam zone (T110)—after annealing at 850 °C.

With a distance increase from Ti-TiB's welded seam zone towards T110, the effect of annealing on structure of welded seam material was not observed. Furthermore, network cells of submicron boride fiber clusters were enlarged gradually in size (see Figure 16) and were not observed in the zone wherein T110 alloy remained in solid state. In the welded joint the boride submicron fibers do not

have predominant directions in the welded seam material, but they are locally oriented predominantly along boundary of their clusters network.

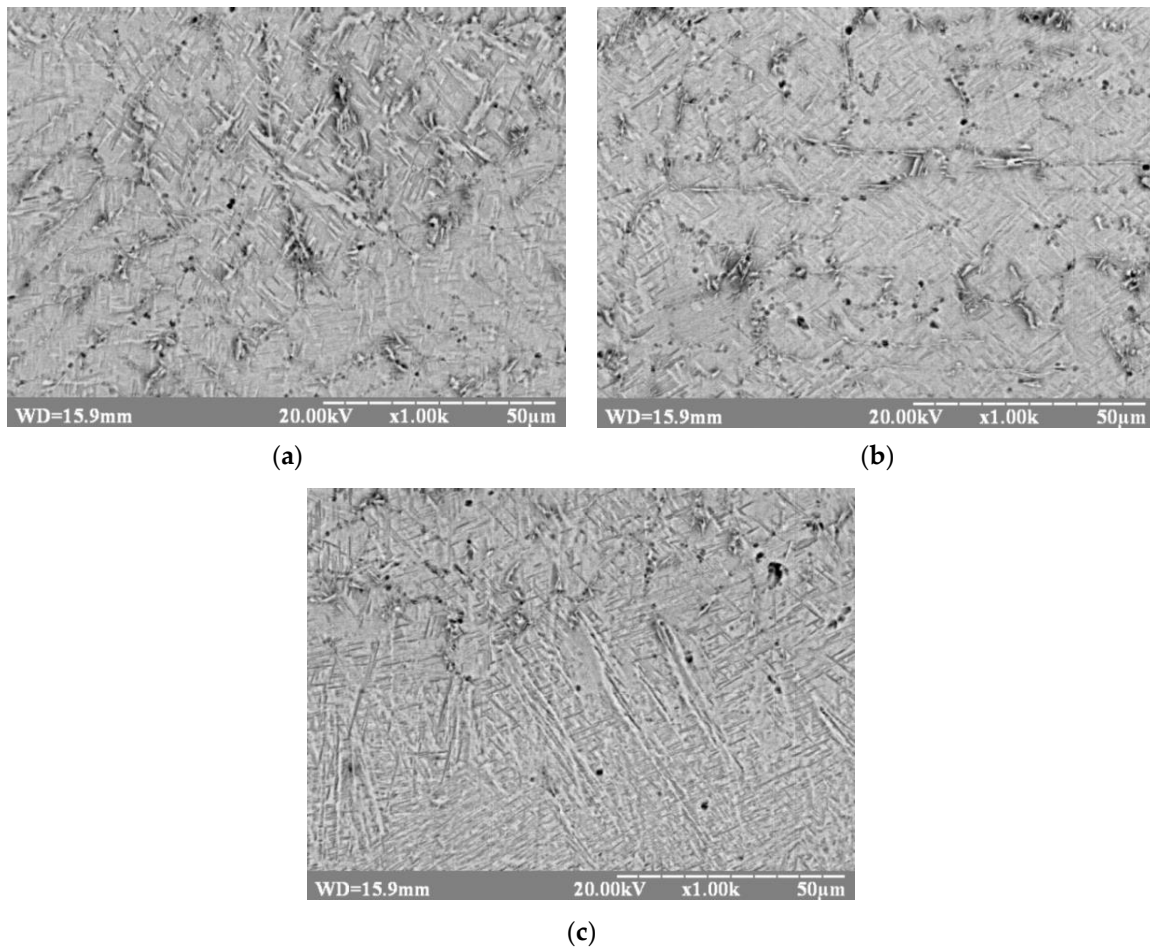


Figure 16. Structure of boride fibers' submicron cluster network with distance from the Ti-TiB—welded seam zone: (a) welded seam zone located from the direction of Ti-TiB—welded seam; (b) welded seam zone located in the middle area; (c) welded seam zone located at the boundary T110 alloy—welded seam (T110 alloy is in the lower part).

X-ray spectral microanalysis of reinforcing fibers in the welded seam zone did not lead to revealing such doped elements in fibers, which are typical for the T110 alloy, besides Al up to 0.18% and Fe up to 0.1%.

During tensile tests conducted at the temperature 20 °C, of the welded Ti-TiB samples (which had an orientation of reinforcing fibers predominantly perpendicular to the plane of the weld butt joint) and T110, fracturing occurred by the base material (Figure 17). With this orientation of the reinforcing fibers, the Ti-TiB alloy was stronger than the T110 alloy, in which fracture occurred. In these cases, the maximum strength with minimum plasticity was observed at the minimum velocity of electron beam movement. The highest level of plasticity was observed at the maximum velocity of electron beam movement and welding of materials initially heated up to 600 °C.

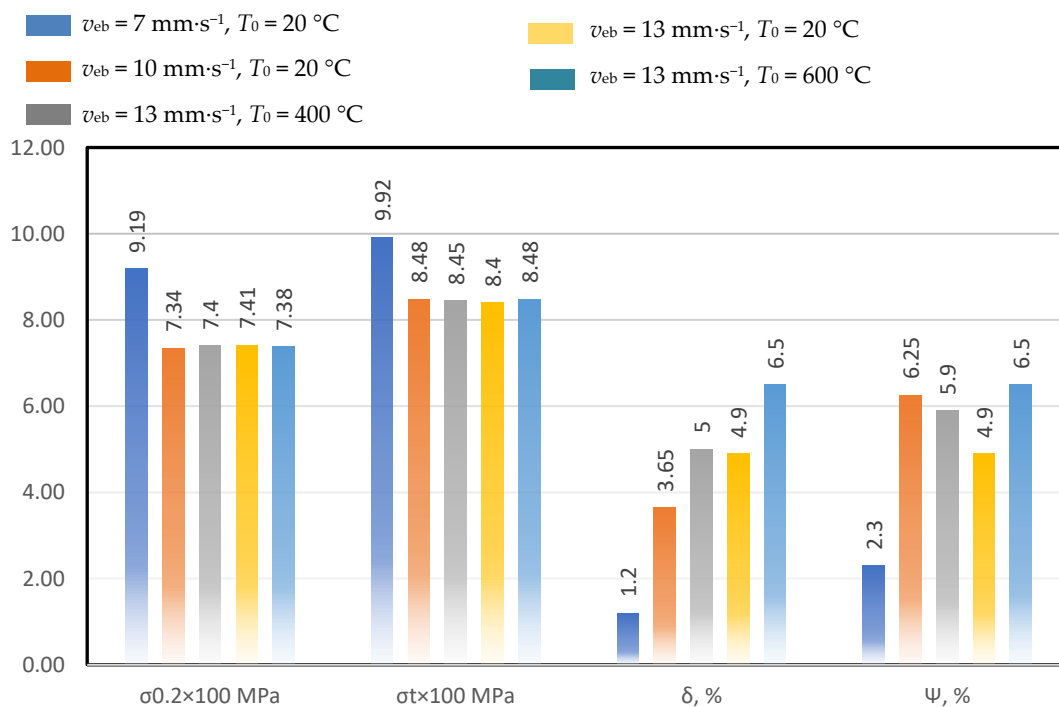


Figure 17. Mechanical properties of (Ti-TiB)-T110 welded joint material obtained under various modes of electron-beam welding.

In order to calculate the strength of the T110 type alloy, by which the fracturing of welded joints took place, the following formula proposed in [22] was used:

$$\sigma_t = 235 + 60 \cdot \iota + 50 \cdot \kappa, \quad (2)$$

where $\iota = \%Al + 0.5\%Sn + 0.33\%Zr + 3.8$, $\kappa = \%Mo + 0.56\%V + 1.25\%Cr + 1.43\%Fe + 0.3\%Nb$.

Calculated σ_t for alloy of T110 type is 1051 MPa according to Equation (2). It matched to the data regarding the strength of T110 alloy quite well ($\sigma_t = 1107 \text{ MPa}$ [23]), and it permits us to consider that the reduced level of strength of this welded joint element is associated with the necessity of after-welding heat treatment.

During the production of the welded joint between Ti-TiB and T110 alloys in the case of minimum electron beam velocity $v_{eb} = 7 \text{ mm}\cdot\text{s}^{-1}$, the dendritic structure typical for Ti-TiB welded seam is retained (see Figure 18a). Under increasing of electron beam velocity, the boride inclusions form a cellular structure. An increase of cell dimensions was also observed for preheated parts ($600 \text{ }^\circ\text{C}$) when compared to parts, welded at the starting temperature of $20 \text{ }^\circ\text{C}$ (see Figure 18).

Enlargement of cells of dendritic-like microstructure upon increase of initial temperature of materials subjected to welding from $20 \text{ }^\circ\text{C}$ to $600 \text{ }^\circ\text{C}$ is probably connected with the incomplete thermodynamic stability of boron-containing areas, adjacent to TiB microfibrers.

In the case of mechanical testing of welded joints between Ti-TiB and T110 alloys, fracturing took place in T110. This proves the higher mechanical properties of weld seam. On the other hand, it demonstrates the necessity of heat treatment optimization in order to increase mechanical properties of welded joints.

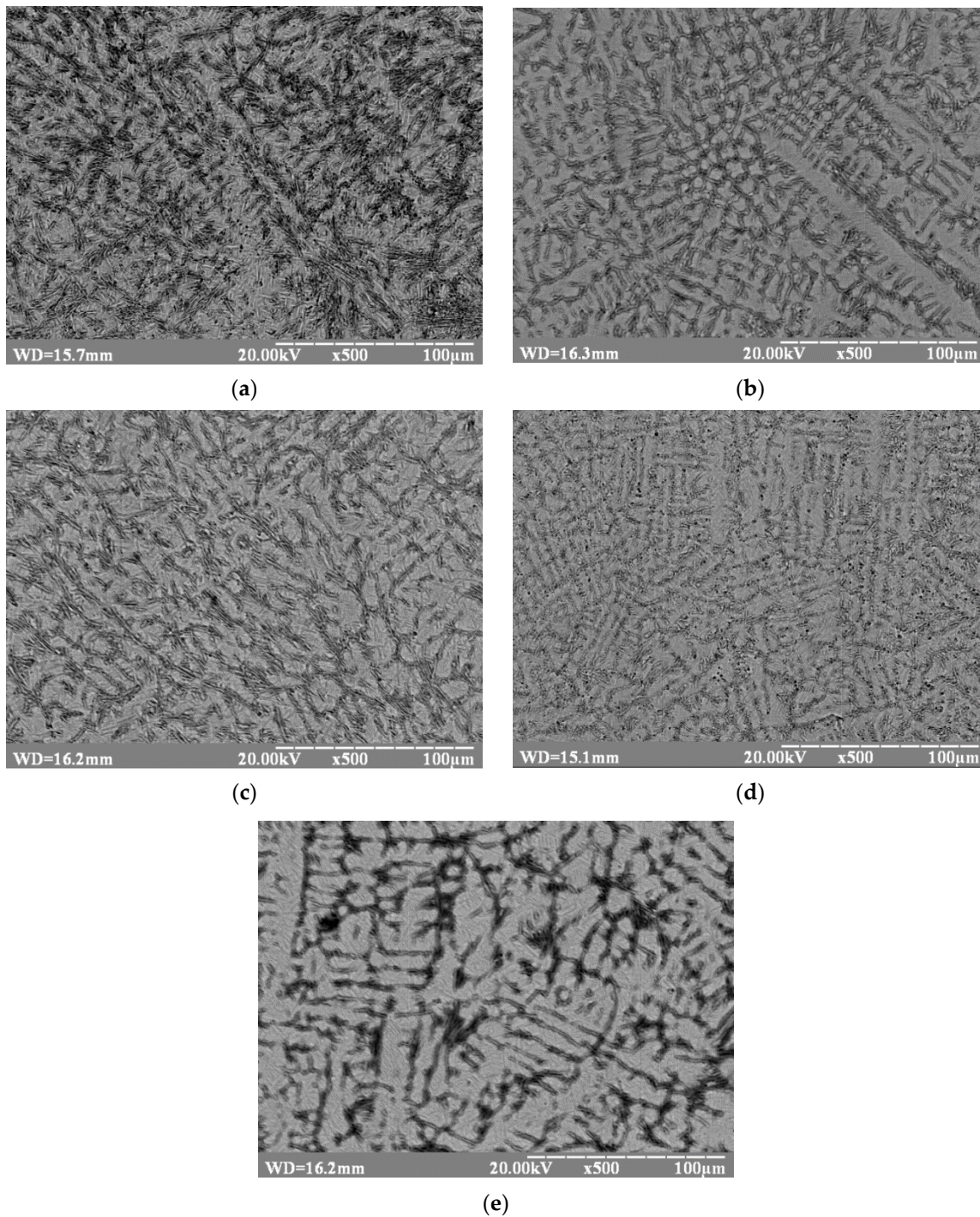


Figure 18. Microstructures of the welded seam material of the (Ti-TiB)-T110 joint: (a) $v_{eb} = 7 \text{ mm}\cdot\text{s}^{-1}$, $T_0 = 20 \text{ }^\circ\text{C}$; (b) $v_{eb} = 10 \text{ mm}\cdot\text{s}^{-1}$, $T_0 = 20 \text{ }^\circ\text{C}$; (c) $v_{eb} = 13 \text{ mm}\cdot\text{s}^{-1}$, $T_0 = 400 \text{ }^\circ\text{C}$; (d) $v_{eb} = 13 \text{ mm}\cdot\text{s}^{-1}$, $T_0 = 20 \text{ }^\circ\text{C}$; (e) $v_{eb} = 13 \text{ mm}\cdot\text{s}^{-1}$, $T_0 = 600 \text{ }^\circ\text{C}$.

Investigation of surface fracturing of a given series of dissimilar welded joints is shown Figure 19a,b. Elements of ductile fracture (light-colored wave combs) are observed on fracture surfaces, and brittle areas correspond, obviously, to the cellular structure areas.

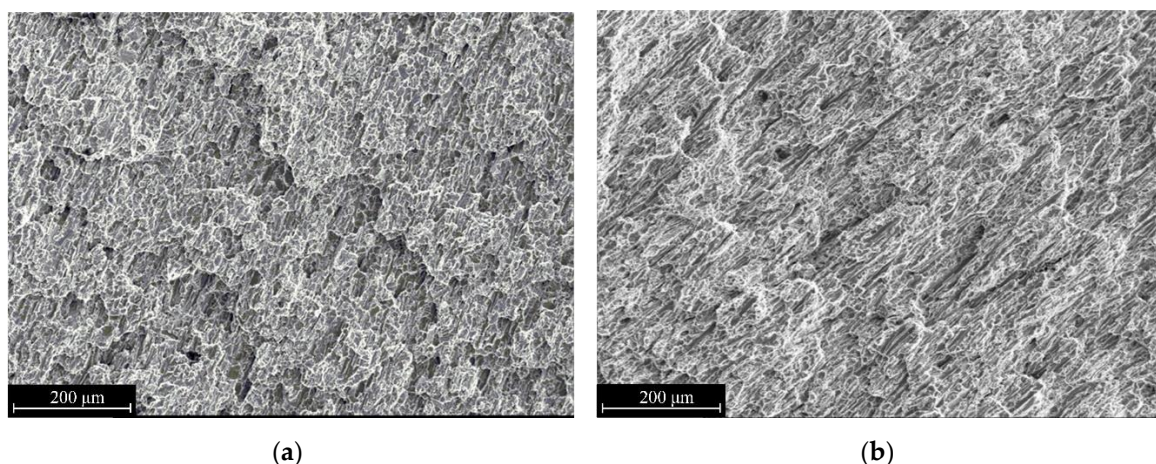


Figure 19. General views of the fracture surfaces of dissimilar welded joints of (Ti-TiB)-T110 series samples at the temperature 20 °C, $\times 100$: (a) plasticity 1.2%; (b) plasticity 4.9%.

Fragmentation of borides absent tearing from the matrix (see the Figure 20) points out the high adhesive strength of the boundary between the titanium matrix and TiB particles. The presence of a boride phase with extremely low plasticity may initiate the development and opening of a brittle crack in the fracture process, which is able to propagate across all of the Ti-TiB material.

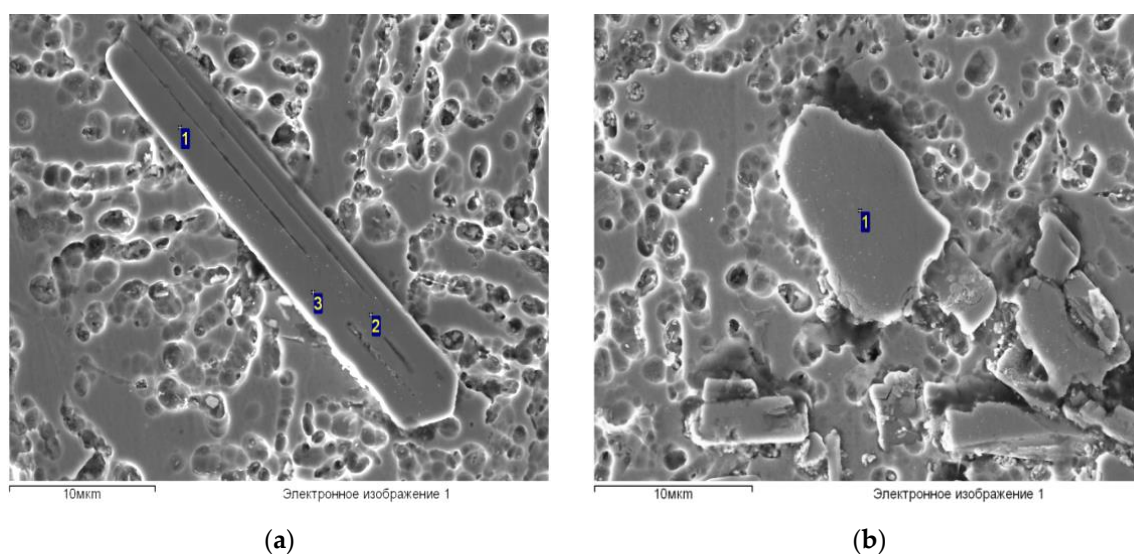


Figure 20. TiB particles in the deformed titanium matrix of the Ti-TiB alloy of a (Ti-TiB)-T110 welded joint: (a) boride plate retained integrity while deforming (TiB_n : $n = 1.47$ (1); 1.01 (2); 1.16 (3)); (b) defragmented boride plate ($n = 1.06$).

During the tensile testing of dissimilar welded joints of Ti-TiB and T110 alloys, produced under low electron beam velocities, a certain level of plasticity was observed: at the minimum electron beam movement velocity of $7 \text{ mm}\cdot\text{s}^{-1}$ it was 1.2%, and at the electron beam movement velocity of $13 \text{ mm}\cdot\text{s}^{-1}$ it was 4.9%, but plasticity increase resulted in strength decrease (see the Figure 19).

Figure 20a,b present the general view of fracture surface of welded joints between (Ti-TiB)-T110 series samples for which a decent level of plasticity is observed under all welding parameters. In this case the fracture surface shows elements of ductile fracture (light-colored wave combs) (see Figure 21), which points to the main crack propagation character (see the Figure 19a). As was mentioned above, in all cases of mechanical testing of (Ti-TiB)-T110 series samples the fracture took place in alloy T110 away from weld seam area.

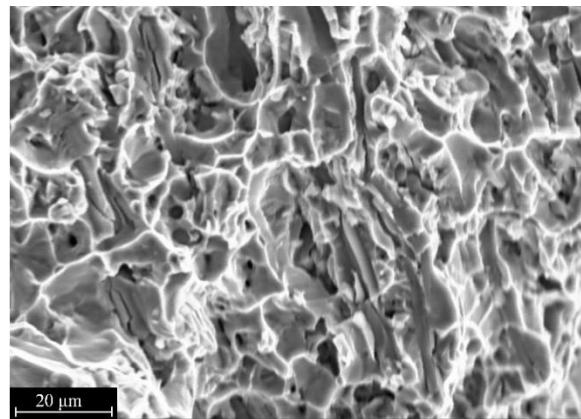


Figure 21. Fragment of ductile fracture of fracture surface of (Ti-TiB)–T110 series samples welded joint at the temperature of subjected to welding samples 600 °C, $\times 1000$.

It should be noted that the conducted fractographic investigations have shown that the fracture surfaces of (Ti-TiB)–T110 series samples demonstrate mixed brittle-ductile fracturing with a prevailing brittle fracture mechanism (see the Figure 22). Increasing of the beam velocity and preheating temperature when welding dissimilar joints, leads to an increase of the ductile fracture fraction. Upon reaching the critical level of stresses in Ti-TiB alloy, large borides are cracked, supposedly due to high stress concentration around them, which results in brittle fracturing (see the Figure 22b). The presence of a larger amount of short borides (less than 5 μm), which are typical for welded seam material, do not result in strong stress localization and thus do not affect the fracture toughness of the plastically deformed matrix.

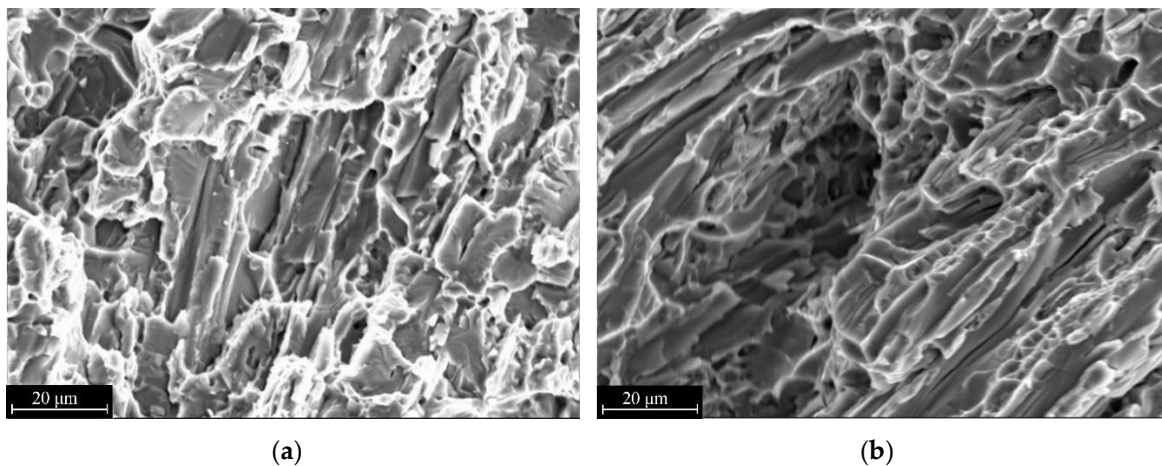


Figure 22. Fragment of ductile fracture of fracture surface of (Ti-TiB)–T110 welded joint, $\times 1000$: (a) $v_{\text{eb}} = 7 \text{ mm}\cdot\text{s}^{-1}$; (b) $v_{\text{eb}} = 13 \text{ mm}\cdot\text{s}^{-1}$.

As mentioned previously, all the specimens fractured in the base metal. This can be explained by the fact that boride fibers' sizes in the weld metal are significantly smaller (TiB fibers ranging from 1 to 20 μm , see Figures 4, 5 and 13–16, and Tables 2–4) compared to the base metal (TiB fibers are between 8 and 70 μm , as shown in Figure 1). Such refinement of boride fibers could possibly lead to higher strength of Ti-TiB, as discussed by Kaczmarek et al. [7]. However, a systematic study with a focus on fiber size variation and distribution and their influence on the mechanical properties of welded joints with a broader range of TiB fiber sizes is needed to check this assumption.

4. Conclusions

1. The electron-beam welding with $U_{acc} = 60$ kV, $I_{eb} = 90$ mA, beam sweep elliptic ($3 \text{ mm} \times 4 \text{ mm}$), transversal, under all values of v_{eb} in the range from 7 to $13 \text{ mm}\cdot\text{s}^{-1}$ ensures production of welded joints of Ti-TiB alloy samples, containing 5 mas. % of TiB_2 in titanium base.
2. During weld seam formation, the basic material is subjected to microstructural changes which result in decreasing of boron-containing fibers thickness from 3–8 μm to 0.1–0.9 μm . Their distinctive initial directionality is lost, and a considerable decrease in the thickness-to-length ratio of the fibers in the boron-containing phase was observed.
3. The transient zone between the base metal and the welded seam material of Ti-TiB alloy has typical dimensions of 40–50 μm . In this zone both the boron-containing fibers of 3–8 μm thickness and 8–40 μm length, typical for an initial material, and thin long boron-containing fibers of 0.1–0.9 μm thickness and 3–15 μm length, typical for a welded seam, were observed.
4. Preheating of welded samples to 400 °C results in a considerable rise of the homogeneity distribution degree of the boron-containing phase in the transient zone and an increase of fiber dimensions of this phase both by length and thickness, both in the transient zone and in the weld metal, compared to non-preheated specimens.
5. Increase of electron beam movement velocity from 7 to $13 \text{ mm}\cdot\text{s}^{-1}$ results in an increase of the transient zone between base material and welded seam material and in a more uniform distribution of boron-containing fibers in titanium matrix.
6. Upon reaching the critical level of tensile stresses, the welded joints of Ti-TiB and T110 type alloys, produced by electron-beam welding under all values of v_{eb} in range from 7 to $13 \text{ mm}\cdot\text{s}^{-1}$ regardless of preheating, are fractured outside of the welded seam zone; the fracture surfaces show signs of mainly brittle fractures.
7. Predominant transversal orientation of TiB-reinforcing fibers in Ti-TiB alloy leads to decrease of mechanical properties of dissimilar joints between Ti-TiB and T110. For such joints, the condition of Ti-TiB alloy is critical, as it is subjected to brittle fracturing. The thermal annealing of the welded joint at the temperature 750 °C (1 h) increases the plasticity of this alloy.

Author Contributions: Conceptualization, P.L. and C.Z.; methodology, E.V. and T.T.; software, V.K.; validation, V.K., T.T. and E.V.; formal analysis, V.Z.; investigation, V.Z., V.K. and T.T.; resources, P.L.; data curation, C.Z.; writing—original draft preparation, V.Z.; writing—review and editing, C.Z.; visualization, V.K. and T.T.; supervision, P.L.; project administration, C.Z.; funding acquisition, P.L. All authors have read and agreed to the published version of the manuscript.

Funding: This research received no external funding.

Conflicts of Interest: The authors declare no conflict of interest.

References

1. Gaisin, R.A.; Imayev, V.M.; Imayev, R.M.; Gaisina, É.R. Microstructure and mechanical properties of VT25U/TiB composite prepared in situ by casting and subjected to hot forging. *Lett. Mater.* **2017**, *7*, 186–196. [[CrossRef](#)]
2. Attar, H.; Bonisch, M.; Calin, M.; Zhang, L.-C.; Scudino, S.; Eckert, J. Selective laser melting of in situ titanium–titanium boride composites: Processing, microstructure and mechanical properties. *Acta Mater.* **2014**, *76*, 13–22. [[CrossRef](#)]
3. Morsi, K.; Patel, V.V. Processing and properties of titanium–titanium boride (TiB) matrix composites—A review. *J. Mater. Sci.* **2007**, *42*, 2037–2047. [[CrossRef](#)]
4. Rahoma, H.K.S.; Wang, X.P.; Kong, F.T.; Chen, Y.Y.; Han, J.C.; Derradji, M. Effect of $(\alpha+\beta)$ heat treatment on microstructure and mechanical properties of (TiB+TiC)/Ti-B20 matrix composite. *Mater. Des.* **2015**, *87*, 488–494. [[CrossRef](#)]
5. García de Cortazar, M.; Agote, I.; Silveira, E.; Egizabal, P.; Coletto, J.; Petitcorps, Y.L. Titanium composite materials for transportation applications. *JOM* **2008**, *60*, 40–46. [[CrossRef](#)]

6. Zhang, J.; Ke, W.; Ji, W.; Fan, Z.; Wang, W.; Fu, Z. Microstructure and properties of insitu titanium boride (TiB)/titanium (Ti) composites. *Mater. Sci. Eng. A* **2015**, *648*, 158–163. [[CrossRef](#)]
7. Kaczmarek, M.; Jurczyk, M.U.; Miklaszewski, A.; Paszel-Jaworska, A.; Romaniuk, A.; Lipińska, N.; Żurawski, J.; Urbaniak, P.; Jurczyk, K. In vitro biocompatibility of titanium after plasma surface alloying with boron. *Mater. Sci. Eng. C* **2016**, *69*, 1240–1247. [[CrossRef](#)] [[PubMed](#)]
8. Vishniakov, L.R.; Grudina, T.V.; Kadyrov, V.K.; Karpinos, D.I.; Oleinik, V.I. *Composition Materials: Reference Book*; Naukova Dumka: Kiev, Ukraine, 1985; 589p. (In Russian)
9. Gaisin, R.A.; Imayev, V.M.; Imayev, R.M. Microstructure and mechanical properties of Ti–TiB based short-fiber composite materials manufactured by casting and subjected to deformation processing. *Russ. Phys. J.* **2015**, *58*, 848–853. [[CrossRef](#)]
10. Elliot, R. *Eutectic Solidification Processing*; Engl. transl.; Shvindlerman, L.S., Ed.; Metallurgy: Moscow, Russia, 1987; 352p. (In Russian)
11. Paton, B.E.; Trigub, N.P.; Akhonin, S.V.; Zhuk, G.V. *Titan Electron-Beam Melting*; Naukova Dumka: Kiev, Ukraine, 2006; 248p, ISBN 966-00-0665-9. (In Russian)
12. Grigorenko, G.M.; Akhonin, S.V.; Loboda, P.I.; Grigorenko, S.G.; Severin, A.Y.; Berezos, V.A.; Bogomol, Y.I. Structure and properties of titanium alloy, alloyed with boron, produced by the method of electron beam remelting. *Electrometall. Today* **2016**, *1*, 21–25. (In Russian) [[CrossRef](#)]
13. Loboda, P.I. *Directionally Crystallized Borides*; Praimdruk: Kyiv, Ukraine, 2012; 395p. (In Ukrainian)
14. Gurevich, S.M.; Zamkov, V.N.; Kompan, Y.Y.; Kushnirenko, N.A.; Kharchenko, G.K.; Blaschuk, V.E.; Volkov, V.B.; Zagrebenyuk, S.D.; Prilutsky, V.P.; Sabokar, V.K. *Metallurgy and Technology of Welding of Titan and Its Alloys*; Zamkov, V.N., Ed.; Naukova Dumka: Kiev, Ukraine, 1986; 240p. (In Russian)
15. Grigorenko, G.M.; Zadorozhnyuk, O.M. Structure, mechanical properties and weldability of pseudo- α and ($\alpha+\beta$)-Ti alloys strengthened by silicides. *Electrometall. Today* **2016**, *2*, 51–56. (In Russian) [[CrossRef](#)]
16. Grabin, V.F. *Fundamentals of Metal Science and Thermal Treatment of Welded Joints from Titanium Alloys*; Naukova Dumka: Kiev, Ukraine, 1975; 262p. (In Russian)
17. Shelyagin, V.D.; Khaskin, V.Y.; Akhonin, S.V.; Belous, V.Y.; Petrichenko, I.K.; Siora, A.V.; Palagesha, A.N.; Selin, R.V. Peculiarities of laser-arc welding of titanium alloys. *Autom. Weld.* **2012**, *12*, 36–40. (In Russian)
18. Nazarenko, O.K.; Kajdalov, A.A.; Kovbasenko, S.N.; Bondarev, A.A.; Shevelev, A.A.; Chvertko, A.I.; Zubchenko, J.V.; Lankin, J.N.; Sheljagin, V.D. *Electron-Beam Welding*; Paton, B.E., Ed.; Naukova Dumka: Kiev, Ukraine, 1987; 255p. (In Russian)
19. Akhonin, S.V.; Belous, V.Y.; Antonyuk, S.L.; Petrichenko, I.K.; Selin, R.V. Properties of high-strength titanium alloy T110 joints made by fusion welding. *Autom. Weld.* **2014**, *1*, 54–57. (In Russian)
20. *State Diagrams of Binary Metal Systems*; Ljakishev, N.P. (Ed.) Mashinostroenie: Moscow, Russia, 1996; Volume 1, 992p, ISBN 5-217-02688-X. (In Russian)
21. Palty, A.E.; Margolin, H.; Nielsen, J.P. Titanium-Nitrogen and Titanium-Boron systems. *Trans. ASM* **1954**, *46*, 312.
22. Khorev, A.I. Fundamental and applied works on titanium alloys and prospective lines of their development. *Technol. Mach. Build.* **2014**, *11*, 5–10. (In Russian)
23. Bychkov, A.S.; Moliar, A.G. Operational load-carrying ability of constructional elements of domestic aircraft of transport category from titanium alloys. *Open Inf. Comput. Integr. Technol.* **2016**, *71*, 18–25. (In Russian)

